Heterogeneous Catalysis

International Edition: DOI: 10.1002/anie.201508113
German Edition: DOI: 10.1002/ange.201508113

Nanostructured Ni_2P as a Robust Catalyst for the Hydrolytic Dehydrogenation of Ammonia–Borane

*Cheng-Yun Peng, Lei Kang, Shuang Cao, Yong Chen, Zhe-Shuai Lin, and Wen-Fu Fu**

Abstract: *Ammonia–borane (AB) is a promising chemical hydrogen-storage material. However, the development of real-time, efficient, controllable, and safe methods for hydrogen release under mild conditions is a challenge in the large-scale use of hydrogen as a long-term solution for future energy security. A new class of low-cost catalytic system is presented that uses nanostructured Ni_2P as catalyst, which exhibits excellent catalytic activity and high sustainability toward hydrolysis of ammonia–borane with the initial turnover frequency of 40.4 $mol_{(H2)} mol_{(Ni2P)}^{-1} min^{-1}$ under air atmosphere and at ambient temperature. This value is higher than those reported for noble-metal-free catalysts, and the obtained Arrhenius activation energy ($E_a = 44.6\ kJ\,mol^{-1}$) for the hydrolysis reaction is comparable to Ru-based bimetallic catalysts. A clearly mechanistic analysis of the hydrolytic reaction of AB based on experimental results and a density functional theory calculation is presented.*

Photocatalytic hydrogen generation from water is an ideal potential solution to the twin problems of global warming and the energy crisis.[1] In the past decade, hydrogen evolution using semiconductor photocatalysts has become a prominent strategy for light-driven proton reduction.[2] However, because of its low boiling point, H_2 is difficult to store in compressed or liquefied form, and this is one of the major challenges in establishing a hydrogen economy. Although many molecular hydride complexes can be used for chemical hydrogen storage, hydrogen capacities of the materials limit their applications.[3] A leading candidate for chemical hydrogen-storage materials, ammonia–borane (H_3NBH_3, AB) has the following advantages: 1) a low molecular weight and high hydrogen content (19.6 wt%, 146 $g\,L^{-1}$); 2) high solubility in water and long-term stability in aqueous solutions and air at room temperature; and 3) non-toxicity.[4] Approaches that combine various catalytic systems consisting of a molecular catalyst,[5] single-metal nanoparticles (NPs),[6] bimetallic NPs,[7] and metal NPs of different sizes and shapes deposited on supports for hydrolysis of AB were proposed; faster H_2-generation rates have been achieved using noble metals or their alloys as catalysts.[8] Nevertheless, considering the wide range of application for the dehydrogenation from molecular hydride and related economic issues, much attention has been paid to the use of earth-abundant metal-based catalysts amongst others for AB hydrolysis.[9] In recent years, although a few highly catalytic efficiency systems of non-noble metal NPs have been developed, NP instability in air or the use of stabilizers and strong reducing agents has limited their commercialization.[10] Xu and co-workers reported that amorphous Fe NPs formed in situ in the presence of AB via reduction of Fe^{2+} with $NaBH_4$ have Pt-like catalytic activity.[11] Jagirdar et al. reported that Co^{2+}, Ni^{2+}, and Cu^{2+} catalyze AB hydrolysis; they verified that the catalysts were metal clusters generated in situ during AB hydrolysis, and that the morphology, size, and dispersion degree of the NPs crucially affect the hydrogen release rates.[9a,12] Recently, common and simple methods have been used to control the sizes and surface morphologies of monometallic NPs, that is, by the addition of other metals to form alloys and core–shell catalysts.[13] Moreover, metal nanocluster catalysts have been distributed and immobilized on various supports such as SiO_2,[14] carbon,[7b,9b,14] carbon nitride,[15] and metal–organic frameworks[16] to provide kinetic control of the catalytic AB hydrolysis reaction. The practice of using bimetallic alloy for various catalytic reactions has witnessed flourishing developments; the catalytic activities of bimetallic NPs are usually significantly higher than those of their monometallic counterparts, as a result of synergistic effects.[17] Recently, an investigation into the mechanism of Pt/carbon nanotube catalytic activity and durability in the hydrolytic dehydrogenation of AB showed that the Pt particle size plays a crucial role in the reaction.[18] Hydrogen release from the hydrolysis of AB using electroless deposition of Co-P/TiO_2 catalyst was reported by Rakap.[19] Although much effort has been made to reduce the costs of catalysts and achieve high dehydrogenation efficiencies in AB hydrolysis for actual applications, the development of AB hydrolysis catalysts that are secure, controllable, inexpensive, highly stable, and sufficiently active under mild conditions is still a challenge.

Nickel phosphide NPs, which consist of inexpensive and earth-abundant elements, and have hollow Ni sites and Ni–P bridging sites, have been extensively investigated as catalysts for electrocatalytic and photocatalytic hydrogen evolution, because of their excellent activity and stability in acid solutions.[20] Here, for the first time, we report a high-activity, stable, secure, and easily prepared Ni_2P NP catalyst for

[*] C.-Y. Peng, Prof. Dr. W.-F. Fu
College of Chemistry and Engineering, Yunnan Normal University
Kunming 650092, (P.R. China)
E-mail: fuwf@mail.ipc.ac.cn

C.-Y. Peng, S. Cao, Prof. Dr. Y. Chen, Prof. Dr. W.-F. Fu
Key Laboratory of Photochemical Conversion and Optoelectronic Materials and HKU-CAS Joint Laboratory on New Materials, Technical Institute of Physics and Chemistry
Chinese Academy of Sciences, Beijing 100190 (P.R. China)

L. Kang, Prof. Dr. Z.-S. Lin
Center for Crystal R&D, Key Lab of Functional Crystals and Laser Technology, Technical Institute of Physics and Chemistry
Chinese Academy of Sciences, Beijing 100190 (P.R. China)

Supporting information for this article is available on the WWW under http://dx.doi.org/10.1002/anie.201508113.

hydrogen release from AB in an ambient atmosphere. The experimental results and a mechanistic interpretation based on density functional theory (DFT) calculations are important for developing a new class of low-cost catalytic system, and provide a more convenient, secure approach to hydrolytic dehydrogenation of substrates.

The Ni_2P NPs were prepared by reacting $Ni(OH)_2$ powder with solid NaH_2PO_2 in argon at 543 K (see the Supporting Information). The NPs were characterized using X-ray diffraction (XRD), energy-dispersive X-ray spectroscopy (EDX), and high-resolution transmission electron microscopy (HRTEM). The four characteristic peaks in the XRD pattern in Figure 1 a can be attributed to the (111), (201), (210), and

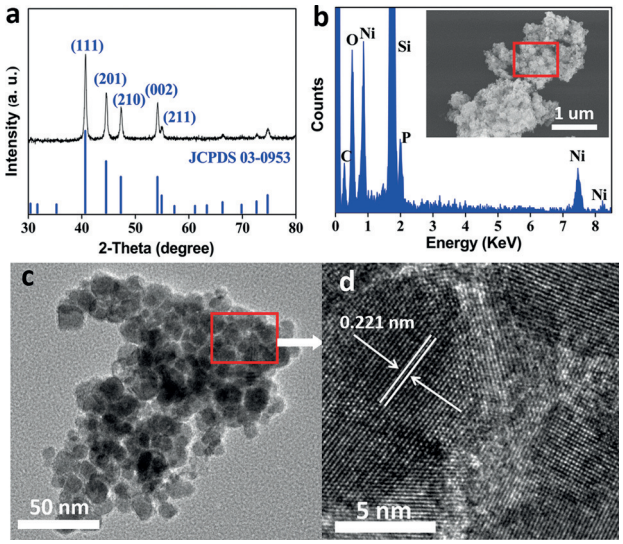

Figure 1. a) XRD pattern and b) EDX results corresponding to a selected scanning electron microscope image (inset); c) TEM and d) HRTEM images of obtained Ni_2P NPs.

(002) crystal planes of Ni_2P (JCPDS No. 03-0953). The EDX results and elemental analysis data obtained by inductively coupled plasma-atomic emission spectrometry show that the atomic ratio of P to Ni is close to 1:2 (Figure 1 b; Supporting Information, Table S1). The TEM image in Figure 1 c shows that the average particle size is less than 12 nm, but indicates agglomerated Ni_2P particles. The Ni_2P NPs are single crystals with faces, as confirmed by the clear lattice fringes with a spacing of 0.221 nm corresponding to the (111) plane of Ni_2P, as depicted in the HRTEM image (Figure 1 d) taken from a region of Figure 1 c. The hydrogen-generating reaction was performed in a closed flask and aerobic atmosphere, with stirring; the volumes of H_2 evolved were determined from the displacement of the water level in a graduated burette (see the Supporting Information).

The activities of various metal phosphides such as FeP, Ni_2P, and Cu_3P in the catalytic hydrolysis of AB were tested (Figure 2; Supporting Information, Figure S1 and S2). The results show that Ni_2P NPs provide a highly efficient, controllable, and robust heterogeneous system for hydrogen release. At room temperature and in the absence of Ni_2P, an AB aqueous solution has long-term stability, without H_2 release.

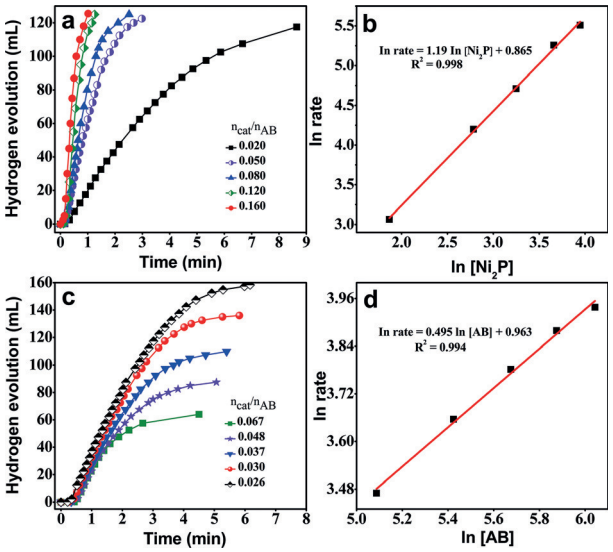

Figure 2. a) Stoichiometric hydrogen evolution in aqueous solution (5 mL) containing fixed amount of AB (1.62 mmol) at various Ni_2P/AB molar ratios at 298 K; c) relationship between hydrogen-generating rate and AB concentration at fixed amount (0.054 mmol) of Ni_2P in water at 298 K; b), d) Logarithmic plots of rate versus [Ni_2P] and [AB], respectively.

We also found that the catalytic activity depends largely on the particle size; the activity of small Ni_2P particles in the initial stage was better than that of larger ones (Supporting Information, Figure S3 and S4). A decrease in the rate of the catalyzed hydrolytic dehydrogenation of AB was observed when sonic oscillation of the catalyst in water was used to reduce the aggregation of Ni_2P particles. This is related to adsorption of H_2O molecules on the active catalyst surface, which hinders the interactions between AB molecules and Ni_2P NPs. This shows that the role of the concentration of the AB aqueous solution in the hydrolytic reaction cannot be neglected.

A kinetic study of AB hydrolysis was performed using a catalyst dispersed in AB aqueous solution (5 mL) under air atmosphere. Small bubbles were released immediately, and the produced gas was identified using gas chromatography (GC-2014C, Shimadzu, with argon as the carrier gas); the amounts were monitored using a water-filled burette. The volumes of gas collected represented nearly stoichiometric amounts of hydrogen, that is, the hydrolysis generated 3 mol of hydrogen gas per mole of AB, meaning that hydrolysis of AB proceed according to Reaction (1):

$$H_3NBH_3 + 2\,H_2O \xrightarrow[rt]{Ni_2P} NH_4^+ + BO_2^- + 3\,H_2 \qquad (1)$$

This is consistent with the data obtained by ^1H NMR and ^{11}B NMR spectra before and after reaction (Supporting Information, Figure S5 and S6). The hydrogen-generating efficiencies of AB aqueous solutions were measured as a function of the Ni_2P catalyst and AB concentrations (Figure 2). The hydrolysis reaction was investigated by varying the Ni_2P/AB molar ratio with either the catalyst or substrate concentration remaining constant at 298 K. Fig-

ure 2a shows that the hydrogen-generating rate depended on $[Ni_2P]$, with less dependence on [AB] (Figure 2c). The hydrolysis of AB (1.62 mmol) at 298 K was completed in the shortest time (61 s) when the amount of Ni_2P was 0.259 mmol, giving initial turnover frequency (TOF) of 39.1 $mol_{(H2)}\,mol_{(Ni2P)}^{-1}\,min^{-1}$. However, the optimum catalytic performance with the highest TOF of 40.4 $mol_{(H2)}\,mol_{(Ni2P)}^{-1}\,min^{-1}$ was achieved at a Ni_2P/AB molar ratio of 0.12; this is comparable to the previously reported performances achieved using noble-metal-free catalysts.[6a,9b,11,21] To the best of our knowledge, this is the highest value ever reported for AB hydrolysis without a noble metal. Figure 2b demonstrates that the logarithmic plot of the calculated initial reaction rate versus catalyst concentration has a slope of 1.19, indicating that the hydrolysis follows first-order kinetics with respect to catalyst concentration. Furthermore, the effect of [AB] on the reaction rate gives important information regarding the nature of the Ni_2P catalyst during the catalytic hydrolysis of AB. As mentioned above, the expected increase in the reaction rate with increasing substrate concentration was observed for the present catalytic system when certain optimization procedures involving the catalyst mass and AB concentration scope were considered, which suggests that this hydrolysis reaction does not follow zero-order kinetics in terms of AB concentration (Figure 2d). This is in good agreement with the results (initiation period and reaction deceleration) observed after sonic oscillation of the catalyst in water, and is well beyond the experimental error limits. This result can be tentatively ascribed to interactions between H_2O and Ni_2P, which impede intimate contact between Ni_2P and AB molecules (see the mechanistic interpretation below).[22]

The temperature dependence of the catalytic reaction was studied in the range 273–323 K, with initial AB and Ni_2P concentrations of 1.62 and 0.054 mmol, respectively; the results are shown in Figure 3a. Control experiments showed that in the absence of Ni_2P, for an aqueous solution of AB placed in a quartz tube and heated at 323 K for 3 h, the volume of hydrogen evolved was less than 4 mL. However, at the same temperature, bubbles were ejected almost instantaneously after the addition of Ni_2P NPs. An Arrhenius plot (inset in Figure 3a) shows that the activation energy for the

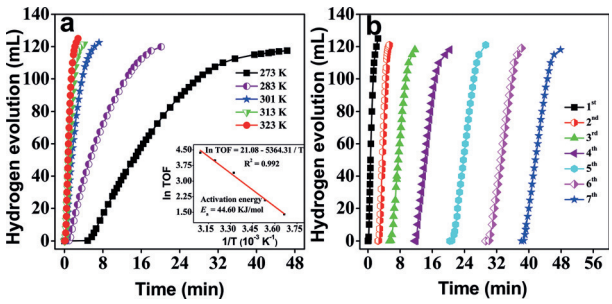

Figure 3. a) Hydrogen-generating rate as a function of temperature in hydrolysis of AB (1.62 mmol) with Ni_2P (0.054 mmol) in water (5 mL). Inset: Arrhenius plot of ln(TOF) versus $1/T$. b) Recycling of Ni_2P catalyst (0.129 mmol) in water (5 mL), with addition of AB (1.62 mmol) to the system in each cycle.

catalytic hydrolysis of AB is 44.6 $kJ\,mol^{-1}$. This value is smaller than the activation energies reported for Ru-based bimetallic catalysts.[13c,23] In practical applications, good reusability and stability of the catalyst are vital. Therefore, hydrolysis experiments were performed in an ambient atmosphere at 298 K to test the catalyst durability; the results (Figure 3b) show that the catalyst had good stability and recyclability. After the seventh cycle (see the Supporting Information), the Ni_2P catalytic activity was still high, and the volume of hydrogen generated was unchanged. However, the hydrogen-generating rate decreased gradually, possibly because of catalyst agglomeration. Envisage was further confirmed by examining surface morphology of the recovered catalyst. The XRD patterns show that the Ni_2P characteristic peaks were still present after many cycles (Supporting Information, Figure S8), X-ray photoelectron spectra also show that the chemical states of Ni and P for Ni_2P NPS before and after catalytic reaction are similar beyond the experimental detection limits (Supporting Information, Figure S7), and atomic ratio of 1:2 for P to Ni was determined through inductively coupled plasma atom emission spectrometry (see the Supporting Information), but the TEM image shows that Ni_2P NP aggregation occurred, which reduced the active surface area of catalyst. This is one reason for the deceleration in hydrogen production (Supporting Information, Figure S9).

To clarify the reaction mechanism, DFT studies were carried out using the CASTEP package[24] with ultrasoft pseudo potentials[25] and the local density approximation[26] to simulate possible reaction pathways for Ni_2P catalysis in AB hydrolysis. Previous studies have shown that the Ni_2P (001) surface is inherently the most stable surface.[20b] This catalyst has moderate interactions with different hydrogen species, originating from a small charge transfer from Ni to P, which results in partially negatively charged P and hydride-acceptor Ni.[27] An investigation of the chemical states of Ni and P for Ni_2P NPS, which was characterized by X-ray photoelectron spectroscopy, shows four peaks around 856.15, 852.79 eV (Ni $2p_{3/2}$) and 873.95, 870.02 eV (Ni $2p_{1/2}$) for the Ni_2P energy levels, corresponding to oxidized nickel species (856.15 and 873.95) and with a very small positive charge $Ni^{\delta+}$ (852.79 and 870.02) in Ni_2P (Supporting Information, Figure S7a,b). Furthermore, the peaks at 133.05 eV and 129.85 (P $2p_{1/2}$), 129.06 eV (P $2p_{3/2}$) are observed, and assigned to oxidized P species and $P^{\delta-}$ arising from charge transfer from Ni to P, respectively (Supporting Information, Figure S7c). This suggests that the presence of P and Ni with different electronic effects on the Ni–P-terminated Ni_2P (001) surface can provide moderate bonding with the substrate to form reaction intermediates, thereby promoting substrate molecular activity, and enhancing the rate of hydrogen evolution. The detailed catalytic hydrolysis mechanism of AB on the Ni_2P surface is shown in Figure 4. As an AB molecule and a water molecule approach the Ni_2P (001) surface (configuration i), the entire system only needs to overcome a very small energy barrier (0.12 eV with the transition state TS-I) to form the intermediate ii. In this configuration, H atoms of B–H group and N–H unit in the AB molecule interact with the Ni atom and the P atoms at the Ni_2P (001) surface, respectively. Meanwhile, the energy of 1.66 eV is released, which provides

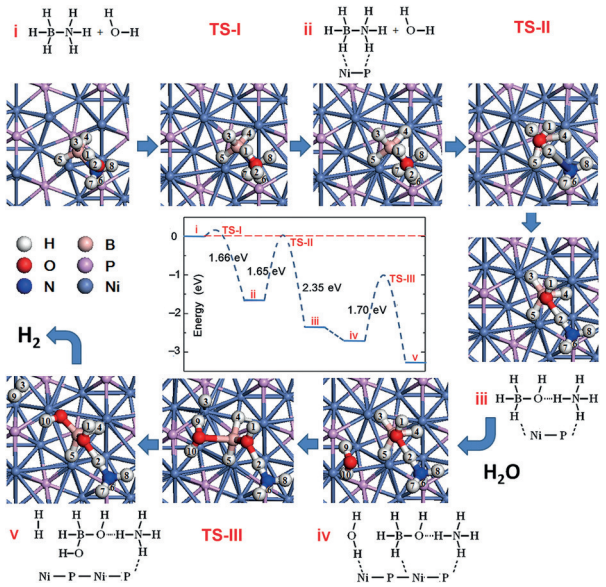

Figure 4. Plot of energy changes versus reaction coordinate calculated for Ni_2P-catalyzed hydrolysis of AB.

the enough active energy to make the O and H atoms in water molecule close to the B and N atoms in the AB molecule to form the transition state II (TS-II) by overcoming the barrier energy of 1.65 eV. In this transition state the B···O and N···H2 distances are 3.933 and 2.740 Å, respectively. Once formed, transition state TS-II proceeds energetically downhill to the intermediate iii, in which the B–O bond length (1.481 Å) and N-H2 distance (1.120 Å) clearly show the presence of H_3BOH^- and NH_4^+, and the B–N bond distance changes from 1.590 in TS-II to 2.833 Å, and the energy of 2.35 eV is released. After production of the intermediate iii, the attack of another adjacent H_2O on the H_3B unit easily generates the intermediate iv without overcoming any energy barrier. By the further evolution from intermediate iv to v with the energy barrier of about 1.70 eV, the H3 atom in the AB molecule and the H9 atom in water molecule can approach each other; and a H_2 molecule can be extracted from the system. Subsequent reactions that the H4 and H5 atoms in the AB molecule can be further released, which would generate two H_2 molecules with other adjacent two water molecules: in total three H_2 molecules can be generated from an AB molecule. It should be noted that along this reaction pathway, the entire process does not need any external energy input, except for a small amount at the initial stage (ca. 0.1 eV), that is, it is almost self-powered. For comparison, we also calculated the energy barriers for $NH_3{-}H_2O{-}BH_3 + H_2O \rightarrow NH_3{-}H_2O{-}BH_2OH + H_2$ (about 6.6 eV) and $NH_3BH_3 + H_2O \rightarrow NH_3BH_2OH + H_2$ (about 9.5 eV) without the catalytic Ni_2P surface. The large reaction barriers reveal that these reaction paths are not favored in the absence of Ni_2P.

In the present study, we achieved the facile, low-cost synthesis of Ni_2P NPs with high catalytic activity and stability in the hydrolytic dehydrogenation of AB, even at a low catalyst content or at 273 K. A maximum activity of 40.4 $mol_{(H2)}\,mol_{(Ni2P)}^{-1}\,min^{-1}$ was achieved under air-saturated atmospheric conditions, which is superior to those of previously reported noble-metal-free systems. These NPs could therefore serve as a high-performance and robust catalyst for the future use of AB as a practical hydrogen-storage material for clean energy applications. Furthermore, an investigation of the mechanism, based on DFT calculations, suggests that the combination of Ni_2P surfaces and substrate molecules significantly enhances the dehydrogenation activity under an ambient atmosphere by reducing the reaction barrier, enabling it to be easily overcome at room temperature.

Acknowledgements

This work was financially supported by the National Key Basic Research Program of China (973 Program 2013CB834804), the Ministry of Science and Technology (2012DFH40090) and 863 Project 2015AA034203. We thank the National Natural Science Foundation of China (21273257, 21267025, 21471155, 11474292 and U1137606) and the Key Research Programme of the Chinese Academy of Science (Grant No. KGZD-EW-T05) for financial support.

Keywords: ammonia–borane · heterogeneous catalysis · hydrogen storage · nickel phosphide · reaction mechanisms

How to cite: *Angew. Chem. Int. Ed.* **2015**, *54*, 15725–15729
Angew. Chem. **2015**, *127*, 15951–15955

[1] a) J. Esswein, D. G. Nocera, *Chem. Rev.* **2007**, *107*, 4022–4047; b) F. E. Osterloh, *Chem. Soc. Rev.* **2013**, *42*, 2294–2320.
[2] a) Z. Han, F. Qiu, R. Eisenberg, P. L. Holland, T. D. Krauss, *Science* **2012**, *338*, 1321–1324; b) J. Liu, Y. Liu, N. Y. Liu, Y. Z. Han, X. Zhang, H. Huang, Y. Lifshitz, S.-T. Lee, J. Zhong, Z. H. Kang, *Science* **2015**, *347*, 970–974.
[3] L. Schlapbach, A. Züttel, *Nature* **2001**, *414*, 353–358.
[4] a) M. Chandra, Q. Xu, *J. Power Sources* **2006**, *156*, 190–194; b) B. Peng, J. Chen, *Energy Environ. Sci.* **2008**, *1*, 479–483; c) Q.-L. Zhu, Q. Xu, *Energy Environ. Sci.* **2015**, *8*, 478–512.
[5] a) X. B. Hu, M. Soleilhavoup, M. Melaimi, J. X. Chu, G. Bertrand, *Angew. Chem. Int. Ed.* **2015**, *54*, 6008–6011; *Angew. Chem.* **2015**, *127*, 6106–6109; b) H. C. Johnson, A. S. Weller, *Angew. Chem. Int. Ed.* **2015**, *54*, 10173–10177; *Angew. Chem.* **2015**, *127*, 10311–10315.
[6] a) Ö. Metin, V. Mazumder, S. Özkar, S. H. Sun, *J. Am. Chem. Soc.* **2010**, *132*, 1468–1469; b) P. Z. Li, A. Aijaz, Q. Xu, *Angew. Chem. Int. Ed.* **2012**, *51*, 6753–6756; *Angew. Chem.* **2012**, *124*, 6857–6860.
[7] a) J. M. Yan, X. B. Zhang, T. Akita, M. Haruta, Q. Xu, *J. Am. Chem. Soc.* **2010**, *132*, 5326–5327; b) L. He, Y. Q. Huang, A. Q. Wang, X. D. Wang, X. W. Chen, J. J. Delgado, T. Zhang, *Angew. Chem. Int. Ed.* **2012**, *51*, 6191–6194; *Angew. Chem.* **2012**, *124*, 6295–6298; c) A. Serov, M. Paddilla, A. J. Roy, P. Atanassov, T. Sakamoto, K. Asazawa, H. Tanaka, *Angew. Chem. Int. Ed.* **2014**, *53*, 10336–10339; *Angew. Chem.* **2014**, *126*, 10504–10507.
[8] a) M. Kaya, M. Zahmakiran, S. Özkar, M. Volkan, *ACS Appl. Mater. Interfaces* **2012**, *4*, 3866–3873; b) H.-L. Jiang, T. Umegaki, T. Akita, X.-B. Zhang, M. Haruta, Q. Xu, *Chem. Eur. J.* **2010**, *16*, 3132–3137; c) O. Ozay, E. Inger, N. Aktas, N. Sahiner, *Int. J. Hydrogen Energy* **2011**, *36*, 8209–8216.
[9] a) S. B. Kalidindi, J. Joseph, B. R. Jagirdar, *Energy Environ. Sci.* **2009**, *2*, 1274–1276; b) G. Q. Zhao, J. Zhong, J. Wang, T.-K. Sham, X. H. Sun, S.-T. Lee, *Nanoscale* **2015**, *7*, 9715–9722; c) M. E. Bluhm, M. G. Bradley, R. Butterick, U. Kusari, L. G. Sneddon, *J. Am. Chem. Soc.* **2006**, *128*, 7748–7749.

[10] a) H.-L. Jiang, T. Akita, Q. Xu, *Chem. Commun.* **2011**, *47*, 10999 – 11001; b) J.-M. Yan, Z.-L. Wang, H.-L. Wang, Q. Jiang, *J. Mater. Chem.* **2012**, *22*, 10990 – 10993; c) L. Yang, J. Su, W. Luo, G. Cheng, *ChemCatChem* **2014**, *6*, 1617 – 1625.
[11] J.-M. Yan, X.-B. Zhang, S. Han, H. Shioyama, Q. Xu, *Angew. Chem. Int. Ed.* **2008**, *47*, 2287 – 2289; *Angew. Chem.* **2008**, *120*, 2319 – 2321.
[12] S. B. Kalidindi, M. Indirani, B. R. Jagirdar, *Inorg. Chem.* **2008**, *47*, 7424 – 7429.
[13] a) A. K. Singh, Q. Xu, *ChemCatChem* **2013**, *5*, 652 – 676; b) D. Su, V. Mazumder, Ö. Metin, S. Sun, *ACS Nano* **2011**, *5*, 6458 – 6464; c) G. Chen, S. Desinan, R. Rosei, F. Rosei, D. Ma, *Chem. Eur. J.* **2012**, *18*, 7925 – 7930.
[14] N. Patel, R. Fernandes, A. Santini, A. Miotello, *Int. J. Hydrogen Energy* **2012**, *37*, 2007 – 2013.
[15] L.-T. Guo, Y.-Y. Cai, J.-M. Ge, Y.-N. Zhang, L.-H. Gong, X.-H. Li, K.-X. Wang, Q.-Z. Ren, J. Su, J. S. Chen, *ACS Catal.* **2015**, *5*, 388 – 392.
[16] a) Q. L. Zhu, J. Li, Q. Xu, *J. Am. Chem. Soc.* **2013**, *135*, 10210 – 10213; b) X. B. Wang, L. H. Xie, K.-W. Huang, Z. P. Lai, *Chem. Commun.* **2015**, *51*, 7610 – 7613.
[17] a) M. Yamauchi, R. Abe, T. Tsukuda, K. Kato, M. Takata, *J. Am. Chem. Soc.* **2011**, *133*, 1150 – 1152; b) S. Guo, S. Zhang, D. Su, S. Sun, *J. Am. Chem. Soc.* **2013**, *135*, 13879 – 13884; c) S. Wang, D. Zhang, Y. Y. Ma, H. Zhang, J. Gao, Y. T. Nie, X. H. Sun, *ACS Appl. Mater. Interfaces* **2014**, *6*, 12429 – 12435.
[18] W. Chen, J. Ji, X. Feng, X. Duan, G. Qian, P. Li, X. Zhou, D. Chen, K. Yuan, *J. Am. Chem. Soc.* **2014**, *136*, 16736 – 16739.
[19] M. J. Rakap, *J. Power Sources* **2014**, *265*, 50 – 56.
[20] a) S. J. Sawhill, D. C. Phillips, M. E. Bussell, *J. Catal.* **2003**, *215*, 208 – 219; b) E. J. Popczun, J. R. McKone, C. G. Read, A. J. Biacchi, A. M. Wiltrout, N. S. Lewis, R. E. Schaak, *J. Am. Chem. Soc.* **2013**, *135*, 9267 – 9270; c) S. Cao, Y. Chen, C. J. Wang, P. He, W. F. Fu, *Chem. Commun.* **2014**, *50*, 10427 – 10429; d) L. Feng, H. Vrubel, M. Bensimon, X. Hu, *Phys. Chem. Chem. Phys.* **2014**, *16*, 5917 – 5921; e) S. Cao, Y. Chen, C. C. Hou, X. J. Lv, W. F. Fu, *J. Mater. Chem. A* **2015**, *3*, 6096 – 6101.
[21] J. T. Hu, Z. X. Chen, M. X. Li, X. H. Zhou, H. B. Lu, *ACS Appl. Mater. Interfaces* **2014**, *6*, 13191 – 13200.
[22] M. Rakap, E. E. Kalu, S. Özkar, *Int. J. Hydrogen Energy* **2011**, *36*, 254 – 261.
[23] a) Ö. Metin, S. Sahin, S. Özkar, *Int. J. Hydrogen Energy* **2009**, *34*, 6304 – 6313; b) N. Mohajeri, A. T-Raissi, O. Adebiyi, *J. Power Sources* **2007**, *167*, 482 – 485.
[24] S. J. Clark, M. D. Segall, C. J. Pickard, P. J. Hasnip, M. J. Probert, K. Refson, M. C. Payne, *Z. Kristallogr.* **2005**, *220*, 567 – 570.
[25] J. S. Lin, A. Qteish, M. C. Payne, V. Heine, *Phys. Rev. B* **1993**, *47*, 4174 – 4180.
[26] D. M. Ceperley, B. J. Alder, *Phys. Rev. Lett.* **1980**, *45*, 566 – 569.
[27] a) Z. P. Huang, Z. B. Chen, Z. Z. Chen, C. C. Lv, H. Meng, C. Zhang, *ACS Nano* **2014**, *8*, 8121 – 8129; b) A. Han, H. L. Chen, Z. J. Sun, J. Xu, P. W. Du, *Chem. Commun.* **2015**, *51*, 11626 – 11629.

Received: August 30, 2015
Published online: November 5, 2015

